

Revised mass-radius relationships for water-rich rocky planets more irradiated than the runaway greenhouse limit.

Martin Turbet¹, Emeline Bolmont¹, David Ehrenreich¹, Pierre Gratier², Jérémy Leconte², Franck Selsis², Nathan Hara¹, Christophe Lovis¹

¹ Observatoire astronomique de l'Université de Genève, 51 chemin des Maillettes, 1290 Sauverny, Switzerland e-mail: martin.turbet@unige.ch

² Laboratoire d'astrophysique de Bordeaux, Univ. Bordeaux, CNRS, B18N, allée Geoffroy Saint-Hilaire, 33615 Pessac, France

Received; accepted

ABSTRACT

Mass-radius relationships for water-rich rocky planets are usually calculated assuming most water is present in condensed (either liquid or solid) form. Planet density estimates are then compared to these mass-radius relationships, even when these planets are more irradiated than the runaway greenhouse irradiation limit (around 1.1 times the insolation at Earth for planets orbiting a Sun-like star), for which water has been shown to be unstable in condensed form and would instead form a thick H₂O-dominated atmosphere. Here we use a 1-D radiative-convective inverse version of the LMD generic numerical climate model to derive new theoretical mass-radius relationships appropriate for water-rich rocky planets that are more irradiated than the runaway greenhouse irradiation limit, meaning planets endowed with a steam, water-dominated atmosphere. As a result of the runaway greenhouse radius inflation effect introduced in previous work, these new mass-radius relationships significantly differ from those traditionally used in the literature. For a given water-to-rock mass ratio, these new mass-radius relationships lead to planet bulk densities much lower than calculated when water is assumed to be in condensed form. In other words, using traditional mass-radius relationships for planets that are more irradiated than the runaway greenhouse irradiation limit tends to dramatically overestimate -possibly by several orders of magnitude- their bulk water content. In particular, this result applies to TRAPPIST-1 b, c, and d, which can accommodate a water mass fraction of at most 2, 0.3 and 0.08%, respectively, assuming planetary core with a terrestrial composition. In addition, we show that significant changes of mass-radius relationships (between planets less and more irradiated than the runaway greenhouse limit) can be used to remove bulk composition degeneracies in multiplanetary systems such as TRAPPIST-1. Broadly speaking, our results demonstrate that non-H₂/He-dominated atmospheres can have a first-order effect on the mass-radius relationships, even for rocky planets receiving moderate irradiation. Finally, we provide an empirical formula for the H₂O steam atmosphere thickness as a function of planet core gravity and radius, water content, and irradiation. This formula can easily be used to construct mass-radius relationships for any water-rich, rocky planet (i.e., with any kind of interior composition ranging from pure iron to pure silicate) more irradiated than the runaway greenhouse irradiation threshold.

Use \titlerunning to supply a shorter title and/or \authorrunning to supply a shorter list of authors.

1. Introduction

With the discovery of the nearby TRAPPIST-1 system (Gillon et al. 2016, 2017; Luger et al. 2017), we now have seven rocky planets in temperate orbits for which both radii (Gillon et al. 2017; Luger et al. 2017; Delrez et al. 2018) and masses (Grimm et al. 2018) have been measured with unprecedented accuracy for planets of this nature. Grimm et al. (2018) and Dorn et al. (2018) compared TRAPPIST-1 planets' bulk density¹ estimates with mass-radius relationships of rocky planets endowed with thick condensed water layers and inferred from the comparison that most of the seven planets are likely enriched in volatiles (e.g., water) up to several tens of percent of planetary mass.

We were motivated by these studies to recalculate mass-radius relationships for water-rich rocky planets in cases where all water is vaporized, forming a thick H₂O-dominated steam atmosphere. This situation has been shown to occur for planets receiving more irradiation from their host star than the theoretical runaway greenhouse irradiation limit (Kasting et al. 1993; Gold-

blatt & Watson 2012; Kopparapu et al. 2013). In the TRAPPIST-1 system, the three innermost planets (TRAPPIST-1 b, c, and d) are thought to receive more irradiation than the theoretical runaway greenhouse irradiation limit for ultra-cool stars (Kopparapu et al. 2013; Wolf 2017; Turbet et al. 2018), even when considering the possible negative feedback of substellar water clouds (Yang et al. 2013; Kopparapu et al. 2016) expected on tidally locked planets.

Traditionally, mass-radius relationships (Seager et al. 2007; Sotin et al. 2007; Grasset et al. 2009; Mordasini et al. 2012; Swift et al. 2012; Zeng & Sasselov 2013; Zeng et al. 2016) for water-rich rocky planets are calculated assuming water is either in solid or liquid form, depending on planet equilibrium temperatures. Some studies (Dorn et al. 2018; Zeng et al. 2019) included the effect of a H₂O-rich atmosphere on the planetary radius estimate by assuming an isothermal steam atmosphere at the equilibrium planet temperature. Thomas & Madhusudhan (2016) explored the effect that a thick H₂O atmosphere may have on the mass-radius relationships of Earth to super-Earth-mass planets. To do this, they used a structural model forced at various surface temperatures and in various pressure-boundary conditions. Their model takes convection processes into account, but lacks a radiative transfer. As a result, the surface temperatures

¹ The densities of TRAPPIST-1 planets were measured with the transit timing variations (TTVs) technique. They are therefore absolute densities, and are thus not affected by inaccuracy on the stellar mass and radius measurements (Grimm et al. 2018).

assumed in Thomas & Madhusudhan (2016) are significantly lower than those calculated self-consistently in the standard atmospheric numerical simulations taking into account the radiative exchanges both in short-wave and long-wave ranges (Kopparapu et al. 2013; Goldblatt et al. 2013; Turbet et al. 2019). Radiative transfer is a necessary component to ensure that atmospheric states have reached top-of-atmosphere radiative balance, and thus describe physically realistic planets.

All the aforementioned approaches most likely underestimate the physical size of a H₂O-dominated steam atmosphere for planets receiving more irradiation than the runaway greenhouse limit (Turbet et al. 2019). Using a 1-D numerical radiative-convective climate model, Turbet et al. (2019) in fact recently showed that water-rich planets receiving more irradiation than the runaway greenhouse irradiation threshold should suffer from a strong atmospheric expansion compared to planets receiving less irradiation than this threshold. The effect, which they named the runaway greenhouse radius inflation effect, originates from the cumulative effect of four distinct causes: (i) a significant increase in the total atmospheric mass; (ii) a significant increase in the atmospheric temperatures; (iii) an increase in optical thickness at low atmospheric pressure; and (iv) a decrease in the mean molecular mass.

To the best of our knowledge, the study of Valencia et al. (2013) is the only work ever to have self-consistently considered the effect of a steam H₂O atmosphere on mass-radius relationships in the Earth to super-Earth mass regime planets. However, this work focused on highly irradiated planets only (around 20 times the insolation at Earth), with the aim of improving our understanding of the nature of the exoplanet GJ 1214b. Although they did not directly calculate mass-radius relationships, Nettelmann et al. 2011 (based on previous results from Miller-Ricci & Fortney 2010) also carried out interior-atmosphere calculations self-consistently taking into account the effect of a H₂O-dominated steam atmosphere to evaluate the possible nature of GJ 1214b. The results of Nettelmann et al. (2011) and Valencia et al. (2013) are qualitatively in agreement (and quantitatively in agreement in the case of GJ 1214b), that planets endowed with a steam H₂O atmosphere have a significantly larger radius than icy or liquid ocean planets, for a given water-to-rock ratio. Thomas & Madhusudhan (2016) also recovered qualitatively similar results, that planets endowed with a steam H₂O atmosphere have a significantly larger radius than icy or liquid ocean planets, for a given water-to-rock ratio.

Here we make use of the 1-D inverse radiative-convective model previously introduced in Turbet et al. (2019), coupled to mass-radius relationships of rocky interiors from Zeng et al. (2016), to produce revised mass-radius relationships for rocky planets in temperate orbits endowed with thick H₂O steam envelopes, as predicted for water-rich planets receiving more irradiation than the runaway greenhouse limit (Turbet et al. 2019). While Turbet et al. (2019) focused on the theoretical and numerical ground of the runaway greenhouse radius inflation, as well as observational tests to detect it in the exoplanet population, here we derive and make available to the community mass-radius relationships aimed at better interpreting the nature of terrestrial-size planets, for which we are beginning to have increasingly accurate measurements of masses and radii.

In Section 2, we describe the method we used to calculate mass-radius relationships for planets endowed with steam, water-dominated atmospheres. These new mass-radius relationships are then presented and discussed in Section 3. Lastly, we present the conclusions of this work and discuss future perspectives in Section 4.

2. Methods

In this section, we describe first the method we used to calculate mass-radius relationships for planets endowed with steam, water-dominated atmospheres. We then provide the empirical mass-radius relationship fitted to these calculations.

2.1. Procedure to derive revised mass-radius relationships

We calculated the mass-radius relationships for water-rich rocky planets that are more irradiated than the runaway greenhouse irradiation limit in four main steps: Firstly, we retrieved mass-radius relationships of dry, rocky planets. In this paper, we chose to use the mass-radius relationships of Zeng et al. (2016)² for (i) pure silicate (MgSiO₃) planets; (ii) terrestrial core composition planets; and (iii) pure-iron (Fe) planets. However, any type of rocky interior composition (from pure iron to pure silicate) could be used.

Secondly, for each set of rocky interior mass M_{core} and radius R_{core} , we calculated the transit thickness $Z_{\text{atmosphere}}$ and the mass $M_{\text{atmosphere}}$ that a pure H₂O atmosphere would have for a wide range of possible water atmospheric pressures, using a 1-D inverse radiative-convective version of the LMD Generic model. The model was adapted in Turbet et al. (2019) to simulate the vertical structure of steam atmospheres, taking into account the condensation of water vapor using a non-dilute moist lapse rate formulation as in Marcq et al. (2017) and a radiative transfer using the water-dominated absorption coefficients of Leconte et al. (2013). For the calculation of the atmospheric profile, the change in gravity with altitude is also taken into account. For more details on the model, we refer the reader to Appendix A of Turbet et al. (2019). This second step is discussed in more detail below.

Thirdly, for each set of rocky interior mass and radius, and for each possible water atmospheric pressure, we calculated the resulting mass M_{planet} and transit radius R_{planet} by using $M_{\text{planet}} = M_{\text{core}} + M_{\text{atmosphere}}$, and assuming that $R_{\text{planet}} = R_{\text{core}} + Z_{\text{atmosphere}}$. In Appendix A, we discuss in detail how the relationship $R_{\text{planet}} = R_{\text{core}} + Z_{\text{atmosphere}}$ – with R_{core} calculated neglecting the effect of the atmosphere – remains valid as soon as the mass of the H₂O-dominated atmosphere is significantly lower than the total mass of the planet.

Lastly, we drew mass-radius relationships for rocky planets with various water-to-rock mass ratios. This last step was performed by carrying out a logarithmic interpolation of the water-to-rock mass ratio for each possible rocky core mass and radius using the array of transit radius calculated for a wide range of possible total H₂O atmospheric pressures³.

The second step of our procedure (i.e., the calculation of $Z_{\text{atmosphere}}$) was achieved through a number of substeps listed below: Firstly, we estimated the surface temperature T_{surf} of a H₂O-dominated steam atmosphere as a function of H₂O atmospheric pressure $P_{\text{H}_2\text{O}}$, surface gravity g and irradiation received by the planet S_{eff} , following the same approach as in Turbet et al. 2019 (Fig. 3). To do this, we first performed 1-D inverse radiative-convective calculations for a wide range of surface temperatures (from 300 to 4300 K), irradiances (roughly from 1 to 40× the irradiation received on Earth), surface gravities (from 2 to 50 m s⁻²), and water vapor pressures (from 2.7×10⁵ to 2.7×10⁹ Pa). We then fit a polynomial (see Methods in Ap-

² User-friendly data is provided on the personal website of Li Zeng (<https://www.cfa.harvard.edu/~lzeng/planetmodels.html>).

³ The mass of the H₂O-dominated atmosphere is calculated by summing the mass of each atmospheric layer in our 1-D radiative-convective model.

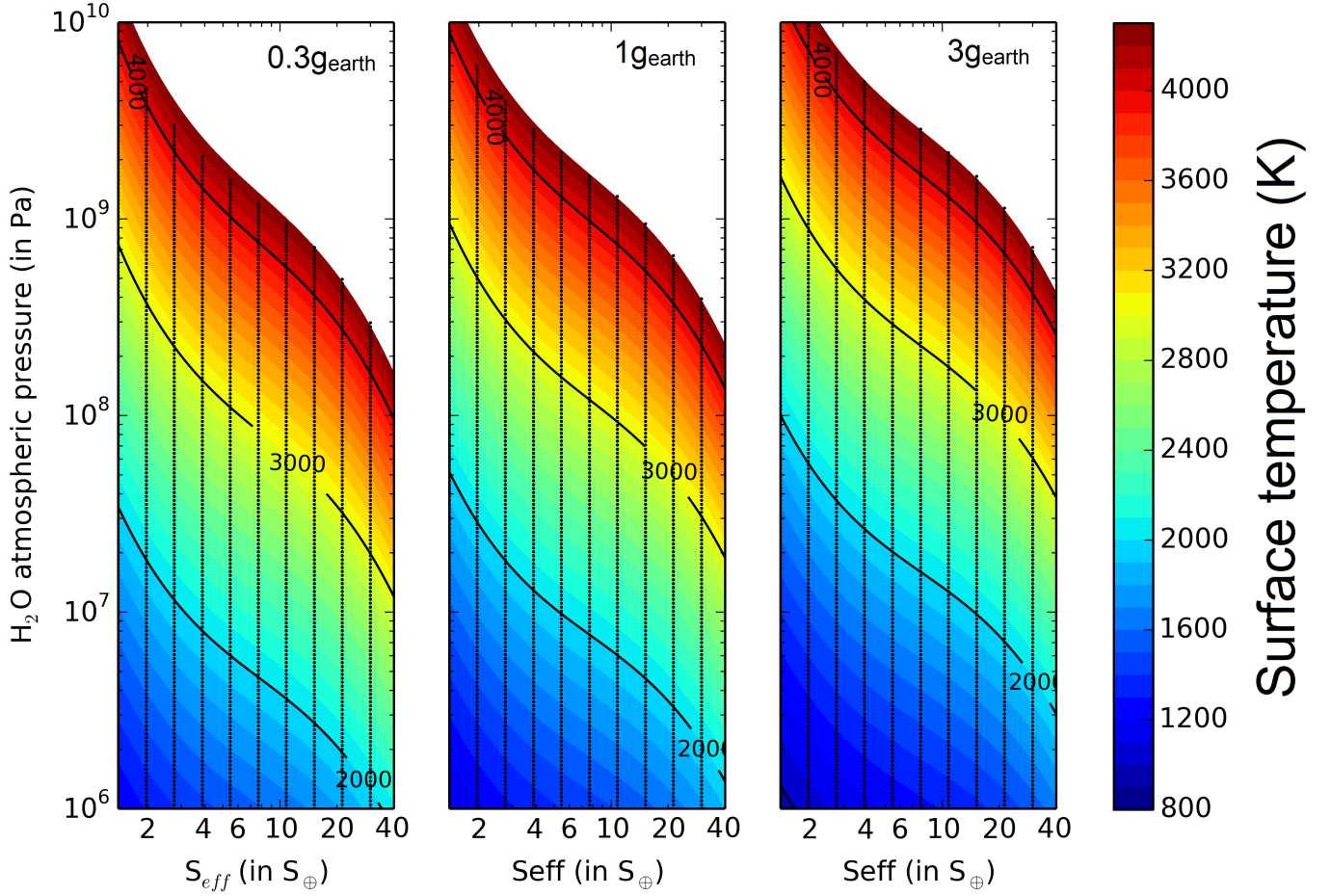


Fig. 1. Surface temperature as a function of the effective flux received on a planet (x-axis) and the surface pressure of its steam H₂O atmosphere (y-axis), for three different surface gravities (0.3, 1 and 3× the gravity on Earth). The surface temperature was estimated using Equation 1. The small black dots indicate the parameter space for which atmospheric numerical simulations have been carried out, and on which the fit of the surface temperature is based.

pendix B) on all these parameters to derive the following empirical equation for the surface temperature T_{surf} (in Kelvins):

$$\log_{10}(T_{\text{surf}}(x, y, z)) = c_1 + c_2 x + c_3 y + c_4 z + c_5 x^2 + c_6 xy + c_7 y^2 + c_8 z^2 + c_9 y^3 + c_{10} z^3, \quad (1)$$

with $x = (\log_{10}(P_{\text{H}_2\text{O}}) - k_1)/k_2$ with $P_{\text{H}_2\text{O}}$ the H₂O partial pressure expressed in bar units, $y = (\log_{10}(g) - k_3)/k_4$ with g the surface gravity (at the interior-atmosphere boundary) in m s^{-2} , and $z = (\log_{10}(S_{\text{eff}}) - k_5)/k_6$ with S_{eff} the irradiation received by the planet (S_{eff} is in Earth insolation units; i.e., $S_{\text{eff}} = 1$ when the planet receives the same insolation as Earth of 1366 W m^{-2}). The empirical coefficients are shown in Table 1.

This empirical relationship provides an estimate of the surface temperature (see Fig 1) of a H₂O-dominated steam atmosphere as a function of surface gravity, water vapor surface pressure and irradiation. It is valid within a few percent for most of the parameter space (maximum error $\sim 10\%$; see Fig. B.2, left panel), for irradiation from ~ 1 to $30 S_{\oplus}$ (assuming the irradiation received by the planet is above the runaway greenhouse irradiation threshold), surface gravity from 0.2 to $6 g_{\oplus}$, and water vapor pressure from 2.7 bar to 27 kbar, and as far as surface temperature remains between 300 and 4300 K.

Secondly, for each possible rocky core mass and radius pair taken from Zeng et al. (2016), and for a wide range of H₂O at-

Table 1. Coefficients for the polynomial fit of the surface temperature of a H₂O steam atmosphere, presented in Equation 1.

Coefficient	Value	Coefficient	Value
k_1	2.688	k_4	4.683×10^{-1}
k_2	1.019	k_5	7.664×10^{-1}
k_3	1.099	k_6	4.224×10^{-1}
c_1	3.401	c_6	8.519×10^{-3}
c_2	1.501×10^{-1}	c_7	-1.467×10^{-2}
c_3	-3.146×10^{-2}	c_8	-7.091×10^{-3}
c_4	4.702×10^{-2}	c_9	-7.627×10^{-3}
c_5	-4.911×10^{-3}	c_{10}	8.348×10^{-3}

mospheric pressures (from 2.7×10^1 to 2.7×10^5 bars), we built the atmospheric structure following the approach presented in Turbet et al. 2019 (Appendix A), and originating from Marcq 2012, Marcq et al. 2017 and Pluriel et al. 2019.

Lastly, we evaluated the transit radius of each possible planet (made of each possible combination of rocky interior and water atmospheric pressure) by integrating these atmospheric profiles in the hydrostatic approximation, using nonideal thermodynamic

properties of H₂O (Haar et al. 1984) as in Turbet et al. 2019, and assuming the transit radius is controlled by the altitude of the upper water cloud layer. For this, we used the altitude of the top of the moist convective layer as a proxy. The total atmospheric transit thickness of a thick H₂O-dominated atmosphere has been shown to be roughly unchanged whether a cloudy or cloud-free atmosphere is considered (Turbet et al. 2019).

2.2. An empirical mass-radius relationship formula

Motivated to make our revised mass-radius relationships accessible to the community, we constructed an empirical mass-radius relationship formula (provided below) for water-rich rocky planets receiving more irradiation than the runaway greenhouse irradiation limit. This formula was constructed in two steps:

Firstly, we derived an analytic expression of the mass-radius relationships, assuming (i) the perfect gas law approximation, and (ii) an isothermal temperature profile:

$$z_{\text{atmosphere}} = \left(\frac{1}{\log \left(\frac{x_{\text{H}_2\text{O}}}{1-x_{\text{H}_2\text{O}}} \times \frac{g_{\text{core}}^2}{4\pi G P_{\text{transit}}} \right) \times \frac{R T_{\text{eff}}}{M_{\text{H}_2\text{O}} g_{\text{core}}} - \frac{1}{R_{\text{core}}} \right)^{-1}, \quad (2)$$

with R_{core} and g_{core} the core (or surface) radius and gravity of the planet, respectively, R the gas constant ($= 8.314 \text{ J K}^{-1} \text{ mol}^{-1}$), $M_{\text{H}_2\text{O}}$ the molar mass of water ($= 1.8 \times 10^{-2} \text{ kg mol}^{-1}$), G the gravitational constant ($= 6.67 \times 10^{-11} \text{ m}^3 \text{ kg}^{-1} \text{ s}^{-2}$), and $x_{\text{H}_2\text{O}}$ the water mass fraction (between 0 and 1) of the planet. P_{transit} is the pressure at the transit radius. T_{eff} is the temperature of the isothermal atmosphere. The procedure to derive this equation is detailed in Appendix C. This equation well describes (see hereafter) the family of possible behaviors of the mass-radius relationships for H₂O steam atmosphere planets.

Secondly, we fit the free parameters (T_{eff} and P_{transit}) using the range of simulations described in the previous subsection. Our simulations show that P_{transit} varies little across the range of parameters we explored and is roughly equal to 10^{-1} Pa . We thus set it to this value. T_{eff} is an effective atmospheric temperature that we empirically fit (see Methods in Appendix B) as follows:

$$\log_{10}(T_{\text{eff}}(x, y, z)) = \beta_1 + \beta_2 x + \beta_3 y + \beta_4 z + \beta_5 x y + \beta_6 y^2 + \beta_7 x^3 + \beta_8 x^2 y + \beta_9 x y^2 + \beta_{10} y^4, \quad (3)$$

with $x = (\log_{10}(x_{\text{H}_2\text{O}}) - \alpha_1)/\alpha_2$, with $x_{\text{H}_2\text{O}}$ the mass water fraction of the planet (between 0 and 1), $y = (\log_{10}(g) - \alpha_3)/\alpha_4$, with g the surface gravity (at the interior-atmosphere boundary) in m s^{-2} , and $z = (\log_{10}(S_{\text{eff}}) - \alpha_5)/\alpha_6$, with S_{eff} the irradiation received by the planet (S_{eff} is in Earth insolation units). The empirical coefficients are shown in Table 2.

These relationships (Equations 2 and 3) are valid within a few percent for most of the parameter space (again, maximum error of $\sim 10\%$; see Fig. B.2, right panel), for irradiation from 1 to $30 S_{\oplus}$ (assuming the irradiation received by the planet is above the runaway greenhouse irradiation threshold), surface gravity from 0.2 to $6 g_{\oplus}$, and water vapor pressure from 2.7 bar to 27 kbar, and as far as surface temperature remains between 300 and 4300 K.

We propose in Appendix D a tutorial on how to use these mass-radius relationships.

Table 2. Coefficients for the polynomial fit of the H₂O steam atmosphere effective temperature presented in equation 3.

Coefficient	Value	Coefficient	Value
α_1	-3.550	α_4	4.683×10^{-1}
α_2	1.310	α_5	7.664×10^{-1}
α_3	1.099	α_6	4.224×10^{-1}
β_1	2.846	β_6	1.736×10^{-2}
β_2	1.555×10^{-1}	β_7	1.859×10^{-2}
β_3	8.777×10^{-2}	β_8	4.314×10^{-2}
β_4	6.045×10^{-2}	β_9	3.393×10^{-2}
β_5	1.143×10^{-2}	β_{10}	-1.034×10^{-2}

3. Results

3.1. Revised mass-radius relationships

The main result of this work is summarized in Figure 2, which shows how mass-radius relationships can vary depending on if water is treated as a condensed layer (Zeng et al. 2016) or as an atmosphere (this work). As a direct consequence of the runaway greenhouse radius inflation introduced in Turbet et al. (2019), mass-radius relationships in the steam atmosphere configuration give -for a given planet mass- a significantly larger radius than in the condensed water configuration. This translates in two main consequences: Firstly, traditional mass-radius relationships (Seager et al. 2007; Sotin et al. 2007; Grasset et al. 2009; Morasini et al. 2012; Swift et al. 2012; Zeng & Sasselov 2013; Zeng et al. 2016) for water-rich rocky planets (i.e. where most water is considered to be in the solid or liquid form) tend to significantly overestimate their bulk density if the planets are more irradiated than the runaway greenhouse irradiation limit. Secondly, comparing these traditional mass-radius relationships for water-rich rocky planets with real planet measured densities tend to overestimate the evaluation of their water-to-rock mass fraction, possibly by several orders of magnitude.

In Equations 2 and 3, we provide an empirical formula for the H₂O steam atmosphere thickness as a function of planet core gravity and radius, water content and irradiation. This formula can easily be used (see the procedure in Appendix D) to construct mass-radius relationships for water-rich, rocky planets that are more irradiated than the runaway greenhouse irradiation threshold, for any type of planet interior.

Lastly, our revised mass-radius relationships for steam planets indicate that small rocky planets ($M_{\text{planet}} \lesssim 0.5 M_{\oplus}$) that are more irradiated than the runaway greenhouse irradiation threshold should be unable to retain more than a few percent water by mass. This is because for these small planets the runaway-greenhouse-induced radius inflation is so extreme that the upper atmosphere becomes gravitationally unbounded for steam atmospheres -only a few percent by mass- and efficient atmospheric escape mechanisms should take place. For instance, for a $0.3 M_{\oplus}$ pure silicate core planet (located just above the runaway greenhouse irradiation threshold) with a 5% water-to-rock ratio, Figure 2 (right panel) indicates that the transit radius lies around $1.2 R_{\oplus}$. The gravity at the transit radius is thus as low as 20% of that at the surface of the Earth, so $\sim 2 \text{ m s}^{-2}$, meaning atmospheric escape can be very strong. In fact, the U-shape of the mass-radius relationships (in the upper-left part of the mass-radius relationships for steam planets in Figure 2) is symptomatic of the fact that the atmosphere becomes gravitationally

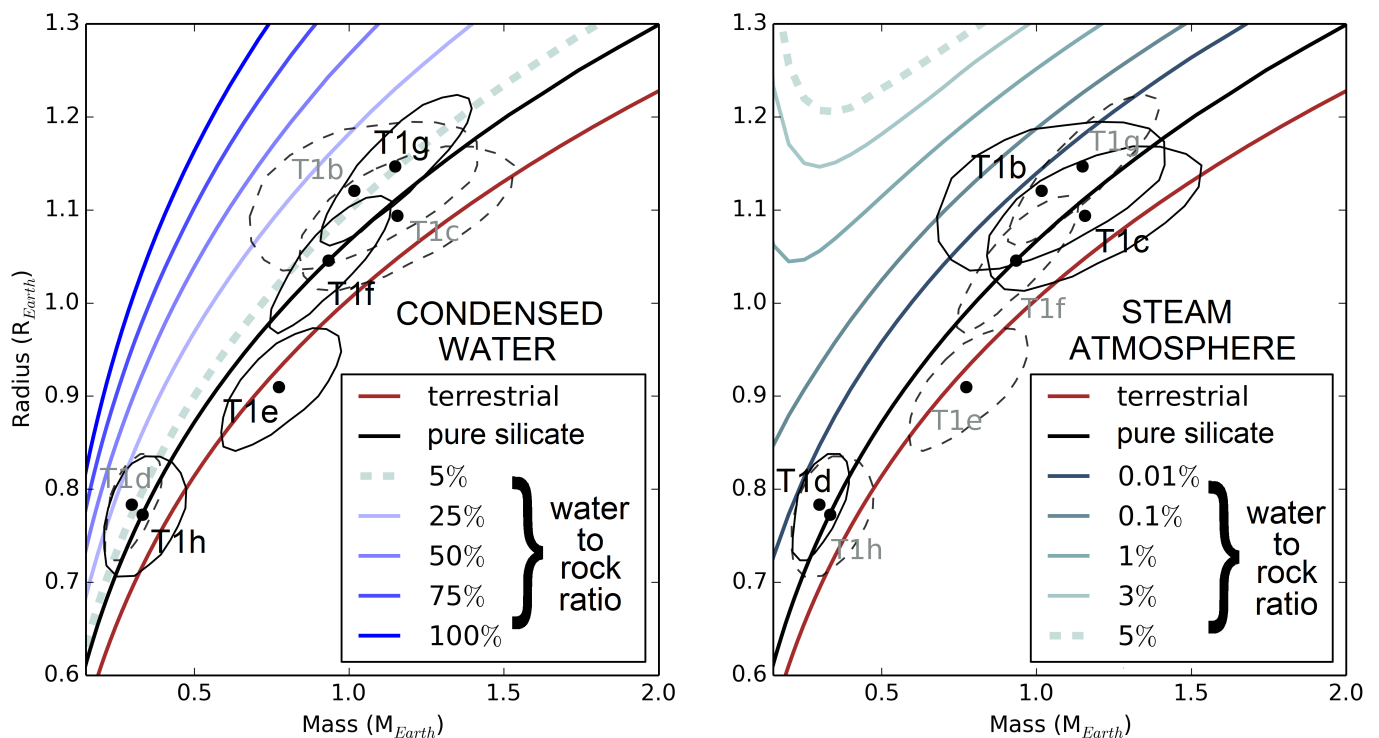


Fig. 2. Mass-radius relationships for various interior compositions and water content, assuming water is in the condensed form (left panel) and water forms an atmosphere (right panel). The silicate composition mass-radius relationship assumes a pure MgSiO_3 interior and was taken from Zeng et al. (2016). The water-rich mass-radius relationships for water in condensed form (left panel) were derived using the data from Zeng et al. (2016). The water-rich mass-radius relationships for water in gaseous form (right panel) are the result of the present work. All mass-radius relationships with water were built assuming a pure MgSiO_3 interior. For comparison, we added the measured positions of the seven TRAPPIST-1 planets measured from Grimm et al. (2018), with their associated 95% confidence ellipses. Based on the irradiation they receive compared to the theoretical runaway greenhouse limit (Kopparapu et al. 2013; Wolf 2017; Turbet et al. 2018), TRAPPIST-1 e, f, g, and h should be compared with mass-radius relationships on the left, while TRAPPIST-1 b, c, and d should be compared with those on the right. To emphasize this, we indicated, on each panel and in black (and solid line ellipses), the planets (and their associated 95% confidence ellipses) for which mass-radius relationships (with water) are appropriate. In contrast, we indicated on each panel in gray (and dashed line ellipses) the planets (and their associated 95% confidence ellipses) for which mass-radius relationships (with water) are not appropriate. For reference, we also added a terrestrial composition that resembles that of the Earth, but also that of Mars and Venus. We note that mass-radius relationships for steam planets (right panel) can be easily built following the procedure described in Appendix D.

unbounded. This U-shape has already been predicted for H_2/He -rich planets (Fortney et al. 2007; Baraffe et al. 2008; Lopez & Fortney 2014; Zeng et al. 2019), but we show here that it is also expected for planets endowed with H_2O -rich atmospheres. This U-shape can be described well at first order by Equation 2.

3.2. Application to the TRAPPIST-1 system

The fact that the use of traditional mass-radius relationships for water-rich rocky planets tend to overestimate the evaluation of a planet water-to-rock mass fraction is particularly relevant for our understanding of the nature of the TRAPPIST-1 planets, the only system known to date (as of November 2019) of temperate-orbit Earth-size planets (Gillon et al. 2017) for which both radii and masses have been measured (Grimm et al. 2018). Based on comparisons of TRAPPIST-1 planet bulk densities with traditional mass-radius relationships, it has been speculated that some planets in the system may be enriched with water, possibly up to tens of percent for some of them (Grimm et al. 2018; Dorn et al. 2018).

Our results suggest that the three innermost planets of the TRAPPIST-1 system -and more particularly, TRAPPIST-1 b and d, for which TTVs measurements point toward particularly low

Table 3. Maximum water content of TRAPPIST-1 b, c, and d, depending on the assumed core composition. Maximum water mass fractions were obtained by finding the corresponding mass-radius relationships that pass just above the 95% confidence ellipses from Grimm et al. (2018).

Core composition	Maximum H_2O mass fraction		
	T-1b	T-1c	T-1d
pure silicate (MgSiO_3)	0.4%	0.01%	0.01%
terrestrial	2%	0.3%	0.08%
pure iron	>10%	>10%	2%

bulk densities (Grimm et al. 2018)- do not necessarily need to be highly enriched with water to reach their measured density. In fact, Table 3 provides quantitative estimates for the maximum water content of the three TRAPPIST-1 innermost planets, for several core compositions. For a core composition similar to that of the solar system terrestrial planets, TRAPPIST-1 b, c, and d cannot accommodate more than 2, 0.3, and 0.08%, respectively, of water. Specifically, TRAPPIST-1 d cannot be composed of more than 2% water whatever the core composition assumed. For comparison, Bourrier et al. (2017) evaluated that the cur-

rent rate of water loss can be as high as 0.19, 0.06, and 0.18% per gigayear by mass for TRAPPIST-1 b, c, and d, respectively. Putting these pieces of information together, it is likely that the three inner TRAPPIST-1 planets may all be completely dry today.

A direct consequence of this result is that if the planets of the TRAPPIST-1 system are all rich in water, as supported by planet formation and migration models for which TRAPPIST-1 planets formed far from their host star, beyond water and other volatile ice lines, and subsequently migrated forming a resonant chain (Ormel et al. 2017; Unterborn et al. 2018; Coleman et al. 2019), then our revised mass-radius relationships -leading to much lower water content for TRAPPIST-1 inner planets than previous calculations (Grimm et al. 2018; Dorn et al. 2018) showed- can be reconciled with the fact that outer planets are expected to be more volatile-rich and water-rich than inner planets (Unterborn et al. 2018), due both to planet formation and migration (Ormel et al. 2017; Unterborn et al. 2018; Coleman et al. 2019), and atmospheric escape processes (Bolmont et al. 2017; Bourrier et al. 2017). This would avoid the need for exotic planet formation and water delivery processes (Dorn et al. 2018; Schoonenberg et al. 2019) to explain apparent density variation with irradiation among TRAPPIST-1 planets.

As of November 2019, the uncertainties on the masses of TRAPPIST-1 planets are still large (see the $2\text{-}\sigma$ uncertainty ellipses on Fig. 2, from Grimm et al. 2018). However, it is expected that these uncertainties will significantly decrease in the near future, either through a follow-up on the transit timing variations (Spitzer Proposal ID 14223, PI: Eric Agol) or using radial velocity measurements with near-infrared ground-based spectrographs (Klein & Donati 2019) such as SPIRou (Artigau et al. 2014) or NIRPS (Wildi et al. 2017).

Below, and with the support of Fig. 3, we discuss, as a proof of concept, one example of a possible scenario for the masses and radii of each of the seven TRAPPIST-1 planets, that of the case where all the TRAPPIST-1 planets closely follow an isocomposition interior mass-radius relationship. The baseline interior composition (10% Fe, 90% MgSiO_3 , i.e., the solid gray line in Fig. 3) was chosen to ensure that this scenario remains compatible with the Grimm et al. (2018) 95% confidence ellipses⁴.

This assumption, however, does not guarantee in principle that the planets do have an interior composition of 10% Fe and 90% MgSiO_3 . This stems from the fact that the composition of the planets is, in principle, highly degenerate, because their positions in the mass-radius diagram (Fig. 3) can be explained either by (i) dry planets with a 10% Fe + 90% MgSiO_3 core (solid gray line in Fig. 3), or (ii) wet planets with a denser core (e.g., 6% water with a terrestrial core, as illustrated by the solid blue line in Fig. 3). This is illustrated in Fig. 3 where the solid blue (6% water with a terrestrial core) and gray (10% Fe + 90% MgSiO_3 core) lines are almost superimposed.

However, this degeneracy is removed here bearing in mind that the three innermost planets of the TRAPPIST-1 system are more irradiated than the runaway greenhouse limit and should therefore follow a different isocomposition mass-radius relationship (e.g., the upper dashed purple line in Fig. 3, for planets with 6% water and a terrestrial core). The black arrows in Fig. 3 indicate the new positions of TRAPPIST-1 b, c, and d in the mass-radius diagram taking into account the revised mass-radius relationship. In other words, the runaway greenhouse transition

allow planets to jump from one mass-radius relationship to another, which makes it possible to break the composition degeneracy.

This demonstrates, to a certain extent, that in our scenario all the TRAPPIST-1 planets should all be very dry, because (i) if all planets were to be water-rich, then they would have to follow a different mass-radius relationship (purple dashed lines for the three innermost planets, versus solid blue line for the four outermost planets in Fig. 3); (ii) if only some of the planets were to be water-rich and others were not, then the planets should not follow an isocomposition mass-radius relationship anyway. In our scenario, we evaluate that, assuming that all TRAPPIST-1 planets have the same mass composition (for the rocky interior and water content), the planets cannot accommodate more than $10^{-3}\%$ of water by mass in order to fit all the small circles in Fig. 3. This argument -that all planets are very dry- should hold unless we are dealing with a fine-tuned scenario where, for each of the planets, all processes (water delivery, runaway greenhouse radius inflation effect, water loss, different core composition) compensate each other exactly.

A direct consequence is that any significant deviation of planetary densities from an interior isocomposition mass-radius relationship would be a strong indication that (i) there is either today large reservoirs of water or volatiles on at least some planets of the system, or that (ii) there are significant differences in TRAPPIST-1 planets' core composition. In some cases (e.g., a significant trend in planets density with irradiation), the first interpretation would be favored.

4. Conclusions

In this work, we calculated revised mass-radius relationships for water-rich, rocky planets, which are more irradiated than the runaway greenhouse irradiation limit. This was performed by coupling the mass-radius relationships for rocky interior of Zeng et al. (2016) with our estimates of the atmospheric thickness of H_2O -dominated atmospheres with a 1-D radiative-convective model.

For a given water-to-rock mass ratio, our revised mass-radius relationships lead to planet bulk densities much lower than calculated when most water is assumed to be in condensed form, which is the common standard in the literature (Seager et al. 2007; Sotin et al. 2007; Grasset et al. 2009; Mordasini et al. 2012; Swift et al. 2012; Zeng & Sasselov 2013; Zeng et al. 2016). This means that using traditional mass-radius relationships for planets that are more irradiated than the runaway greenhouse irradiation limit tends to dramatically overestimate -possibly by several orders of magnitude- their bulk water content.

More specifically, this result has important consequences for our understanding of the nature of the TRAPPIST-1 planets. Our work shows that the measured density (yet to be confirmed) of the three innermost planets of the TRAPPIST-1 system indicates their bulk water content should be significantly lower than what was previously speculated in Grimm et al. (2018) and Dorn et al. (2018). More generally, these results demonstrate that non- H_2/He -dominated atmospheres can have a first-order effect on the mass-radius relationships even for Earth-mass planets receiving moderate irradiation.

Future work should focus on more carefully taking into account possible interactions and feedback between the planet interior and the steam atmosphere, and should aim to extend our work to more irradiated, more massive planets (so-called super-Earth planets), for which mass and radius measurements have

⁴ Note that this condition requires having a core composition of at least $\sim 90\%$ silicate (MgSiO_3).

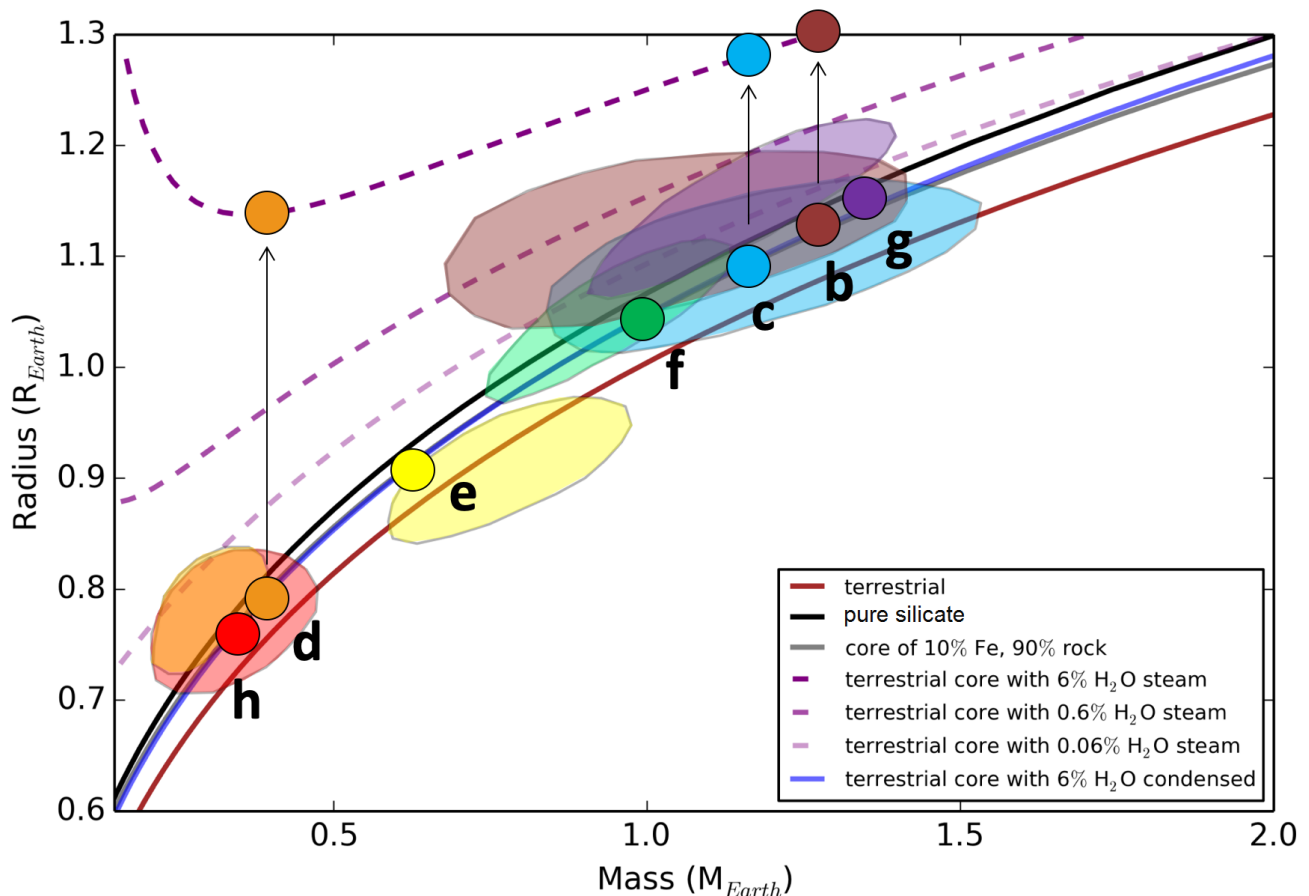


Fig. 3. Example of a scenario for TRAPPIST-1 planets where masses and radii follow an interior isocomposition line (gray line; 10% Fe, 90% MgSiO₃ composition) chosen to be consistent with $2\text{-}\sigma$ uncertainty ellipses of Grimm et al. 2018. While the seven large ellipses indicate the known current estimates (95% confidence) for the masses and radii of the seven TRAPPIST-1 planets, the seven small circles indicate the positions (in the mass, radius diagram) of the seven planets as speculated in our scenario. Each planet (associated with a current uncertainty ellipse, and a speculated position) is identified by a distinct color. This figure also shows mass-radius relationships for terrestrial core planets, in some cases endowed with either a condensed layer of water (solid blue line) or a steam H₂O atmosphere of various masses (dashed purple lines). The mass-radius relationships for steam planets can be built following the procedure described in Appendix D. We note that the mass-radius relationships for steam H₂O-rich atmosphere planets can slightly change depending on the level of stellar irradiation they receive. However, because these changes are low (for the levels of irradiation on TRAPPIST-1 b, c, and d) compared to the runaway-greenhouse-transition-induced mass-radius relationship change, we decided not to show them for clarity.

been performed for a much larger number of planets. For this, an interior model could be coupled to a steam atmosphere model to account for (1) the greenhouse effect feedback of the atmosphere on the interior structure; (2) the planetary core cooling; and (3) the possible outgassing or accumulation through photodissociation of various gases such as O₂, N₂, CO₂, etc. Future work should also re-examine our results with 3-D global climate models, consistently taking into account the effect of clouds and short-wave absorption in the upper atmosphere. This is in order to improve the estimate of the thermal structure and thus the true radius of the planet. Meanwhile, in Section 2 we provide empirical formulae for the surface temperature and the thickness of a H₂O steam atmosphere, as well as a tutorial on how to correctly use them in Appendix D. These formulae can be used in interior models to better capture the boundary effect of a thick H₂O-dominated atmosphere.

Acknowledgements. This project has received funding from the European Union’s Horizon 2020 research and innovation program under the Marie Skłodowska-Curie Grant Agreement No. 832738/ESCAPE. This project has received funding from the European Research Council (ERC) under the European

Union’s Horizon 2020 research and innovation program (grant agreement No. 724427/FOUR ACES and No. 679030/WHIPLASH). This work has been carried out within the framework of the National Centre of Competence in Research PlanetS supported by the Swiss National Science Foundation. The authors acknowledge the financial support of the SNSF. M.T. is grateful for the computing resources on OCCIGEN (CINES, French National HPC). This research has made use of NASA’s Astrophysics Data System. M.T. thanks the Gruber Foundation for its generous support to this research. M.T. thanks Brice-Olivier Demory for providing useful feedbacks on the manuscript. Last but not least, we thank the reviewer for his/her insightful remarks and comments on our manuscript.

References

- Artigau, É., Kouach, D., Donati, J.-F., et al. 2014, in Proceedings of the SPIE, Vol. 9147, Ground-based and Airborne Instrumentation for Astronomy V, 914715
- Baraffe, I., Chabrier, G., & Barman, T. 2008, *Astronomy and Astrophysics*, 482, 315
- Bolmont, E., Selsis, F., Owen, J. E., et al. 2017, *Monthly Notices of the Royal Astronomical Society*, 464, 3728
- Bourrier, V., de Wit, J., Bolmont, E., et al. 2017, *The Astronomical Journal*, 154, 121

- Bower, D. J., Kitzmann, D., Wolf, A. S., et al. 2019, *Astronomy & Astrophysics*, 631, A103
- Coleman, G. A. L., Leleu, A., Alibert, Y., & Benz, W. 2019, *Astronomy & Astrophysics*, 631, A7
- Delrez, L., Gillon, M., Triaud, A. H. M. J., et al. 2018, *Monthly Notices of the Royal Astronomical Society*, 475, 3577
- Dorn, C., Mosegaard, K., Grimm, S. L., & Alibert, Y. 2018, *The Astrophysical Journal*, 865, 20
- Fortney, J. J., Marley, M. S., & Barnes, J. W. 2007, *ApJ*, 659, 1661
- Gillon, M., Jehin, E., Lederer, S. M., et al. 2016, *Nature*, 533, 221
- Gillon, M., Triaud, A. H. M. J., Demory, B.-O., et al. 2017, *Nature*, 542, 456
- Goldblatt, C., Robinson, T. D., Zahnle, K. J., & Crisp, D. 2013, *Nature Geoscience*, 6, 661
- Goldblatt, C. & Watson, A. J. 2012, *Philosophical Transactions of the Royal Society of London Series A*, 370, 4197
- Grasset, O., Schneider, J., & Sotin, C. 2009, *The Astrophysical Journal*, 693, 722
- Grimm, S. L., Demory, B.-O., Gillon, M., et al. 2018, *Astronomy and Astrophysics*, 613, A68
- Haar, L., Gallagher, J., & Kell, G. 1984, *NBS/NRC steam tables thermodynamic and transport properties and computer programs for vapor and liquid states of water in SI units* (Hemisphere Publ. Corp., Washington, D. C.)
- Kasting, J. F., Whitmire, D. P., & Reynolds, R. T. 1993, *Icarus*, 101, 108
- Klein, B. & Donati, J. F. 2019, *Monthly Notices of the Royal Astronomical Society*, 488, 5114
- Kopparapu, R. K., Ramirez, R., Kasting, J. F., et al. 2013, *The Astrophysical Journal*, 765, 131
- Kopparapu, R. K., Ramirez, R. M., Schottelkotte, J., et al. 2014, *The Astrophysical Journal Letters*, 787, L29
- Kopparapu, R. K., Wolf, E. T., Haqq-Misra, J., et al. 2016, *The Astrophysical Journal*, 819, 84
- Leconte, J., Forget, F., Charnay, B., Wordsworth, R., & Pottier, A. 2013, *Nature*, 504, 268
- Lopez, E. D. & Fortney, J. J. 2014, *The Astrophysical Journal*, 792, 1
- Luger, R., Sestovic, M., Kruse, E., et al. 2017, *Nature Astronomy*, 1, 0129
- Marcq, E. 2012, *Journal of Geophysical Research (Planets)*, 117, E01001
- Marcq, E., Salvador, A., Massol, H., & Davaille, A. 2017, *Journal of Geophysical Research (Planets)*, 122, 1539
- Miller-Ricci, E. & Fortney, J. J. 2010, *The Astrophysical Journal Letters*, 716, L74
- Mordasini, C., Alibert, Y., Georgy, C., et al. 2012, *Astronomy & Astrophysics*, 547, A112
- Nettelmann, N., Fortney, J. J., Kramm, U., & Redmer, R. 2011, *The Astrophysical Journal*, 733, 2
- Ormel, C. W., Liu, B., & Schoonenberg, D. 2017, *Astronomy & Astrophysics*, 604, A1
- Pedregosa, F., Varoquaux, G., Gramfort, A., et al. 2011, *Journal of machine learning research*, 12, 2825
- Pluriel, W., Marcq, E., & Turbet, M. 2019, *Icarus*, 317, 583
- Schoonenberg, D., Liu, B., Ormel, C. W., & Dorn, C. 2019, *A&A*, 627, A149
- Seager, S., Kuchner, M., Hier-Majumder, C. A., & Militzer, B. 2007, *The Astrophysical Journal*, 669, 1279
- Sotin, C., Grasset, O., & Mocquet, A. 2007, *Icarus*, 191, 337
- Swift, D. C., Eggert, J. H., Hicks, D. G., et al. 2012, *The Astrophysical Journal*, 744, 59
- Thomas, S. W. & Madhusudhan, N. 2016, *Monthly Notices of the Royal Astronomical Society*, 458, 1330
- Turbet, M., Bolmont, E., Leconte, J., et al. 2018, *Astronomy & Astrophysics*, 612, A86
- Turbet, M., Ehrenreich, D., Lovis, C., Bolmont, E., & Fauchez, T. 2019, *A&A*, 628, A12
- Unterborn, C. T., Desch, S. J., Hinkel, N. R., & Lorenzo, A. 2018, *Nature Astronomy*, 2, 297
- Valencia, D., Guillot, T., Parmentier, V., & Freedman, R. S. 2013, *The Astrophysical Journal*, 775, 10
- Wildi, F., Blind, N., Reshetov, V., et al. 2017, in *Society of Photo-Optical Instrumentation Engineers (SPIE) Conference Series*, Vol. 10400, Society of Photo-Optical Instrumentation Engineers (SPIE) Conference Series, 1040018
- Wolf, E. T. 2017, *The Astrophysical Journal Letters*, 839, L1
- Yang, J., Cowan, N. B., & Abbot, D. S. 2013, *The Astrophysical Journal Letters*, 771, L45
- Zeng, L., Jacobsen, S. B., Sasselov, D. D., et al. 2019, *Proceedings of the National Academy of Science*, 116, 9723
- Zeng, L. & Sasselov, D. 2013, *Publications of the Astronomical Society of the Pacific*, 125, 227
- Zeng, L. & Sasselov, D. 2014, *The Astrophysical Journal*, 784, 96
- Zeng, L., Sasselov, D. D., & Jacobsen, S. B. 2016, *The Astrophysical Journal*, 819, 127

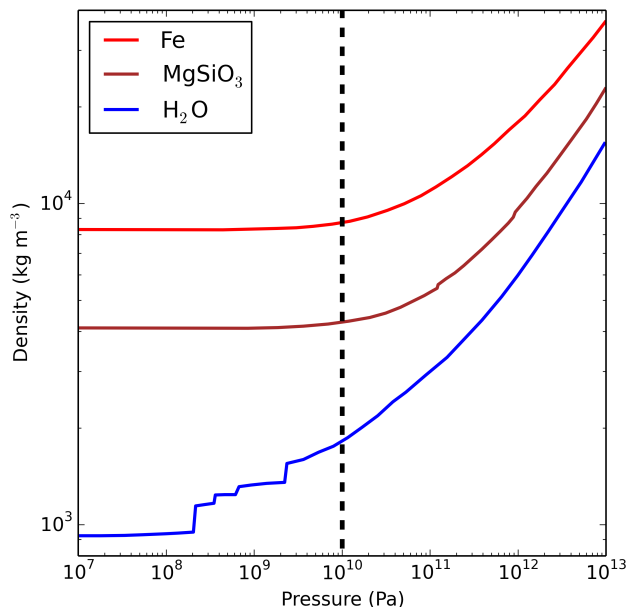


Fig. A.1. Equations of state (EOS) for iron, silicate (MgSiO_3 ; perovskite phase and its high-pressure derivatives), and H_2O (Ice Ih, Ice III, Ice V, Ice VI, Ice VII, Ice X, and superionic phase along its melting curve, i.e., solid-liquid phase boundary). These EOS were taken from Zeng & Sasselov 2013 (Figure 1). The vertical, dashed line denotes the typical pressure at which the density of iron and MgSiO_3 starts to deviate from a constant value.

Appendix A: Why and when the

$R_{\text{planet}} = R_{\text{core}} + Z_{\text{atmosphere}}$ approximation is valid

In order to calculate mass-radius relationships for water-rich rocky planets, we assumed that the transit radius of a planet can be approximated by the sum of the core radius (directly taken from the Zeng et al. 2016 dry mass-radius relationships) and the thickness of the water layer, calculated independently. This approach remains valid only if the feedback of the water layer on the rocky interior physical size is negligible. The presence of a water layer (in solid, liquid, or gaseous form) can have two distinct impacts:

1. The water layer can exert a pressure force that compresses the rocky interior. Figure A.1 shows the equation of state (EOS) for silicate (MgSiO_3 , denoted by a solid brown line). The density of MgSiO_3 is roughly constant until pressure reaches $\sim 10^{10}$ Pascals (denoted by the vertical, dashed line). In other words, it means that if the water layer exerts a basal pressure that is significantly lower than this $\sim 10^{10}$ Pascals limit, then the presence of the water layer should have a negligible effect on the silicate interior density profile and thus its physical size. To check that this effect does not significantly affect the mass-radius relationships presented in Figure 2, we calculated mass-radius relationships of water-rich planets with a pure silicate interior, with water assumed to be present in a solid layer (using the water EOS shown in Figure A.1, denoted by a solid blue line), and compared these calculations with those of Zeng et al. (2016) that self-consistently take into account the pressure feedback on the interior. The result of this comparison is shown in Figure A.2. For a 5% water-to-rock mass ratio, the approximation made in our work leads to a 1% error maximum (for a $2 M_{\oplus}$ core planet) for the range of planets discussed in Figures 2 and A.2. Finally, this demonstrates that the approximation discussed here is largely acceptable to establish the mass-radius relationships presented in Figure 2.
2. The water layer can change the thermal structure and possibly even the physical state of the interior. This is particularly relevant in the H_2O steam atmosphere case where the surface temperature can reach thousands of Kelvin (Kopparapu et al. 2013; Goldblatt et al. 2013; Turbet et al. 2019), which imposes an extreme surface boundary condition on the interior. While the direct interior temperature profile change should have a limited impact on the radius of the rocky core (Seager et al. 2007; Zeng & Sasselov 2014), the temperature change could lead to a phase change of the interior (e.g., melting) that could significantly increase its physical radius (Bower et al. 2019). Taking this effect into account in a self-consistent way requires the use of an interior atmosphere coupled model. We leave this for future work.

Appendix B: Procedure for the polynomial fits

The polynomial fit of our data (surface temperature and effective temperature) was performed in four distinct steps and makes use of the scikit-learn python library (Pedregosa et al. 2011).

As a first step, we recentered and normalized the distribution of values for each parameter (water pressure or water content, surface gravity, stellar flux) of the fit. For this, we used the *StandardScaler* python tool⁵. As a second step, we built a matrix of all possible terms of polynomials of degree n or lower. This matrix was constructed using the *PolynomialFeatures* python tool⁶. As a reminder, for a polynomial of degree n constructed on k

parameters, there is a total number of $N = \binom{k+n}{n} = \frac{(k+n)!}{n!k!}$ polynomial terms. In practice, we constructed a matrix of all possible terms of polynomials of degree $n = 8$ and lower (on our $k = 3$ parameters; i.e., for water pressure or water content, surface gravity, and stellar flux), reaching a total of $N = \binom{3+8}{8} = 165$ polynomial terms for $n = 8$.

⁵ <https://scikit-learn.org/stable/modules/generated/sklearn.preprocessing.StandardScaler.html>

⁶ <https://scikit-learn.org/stable/modules/generated/sklearn.preprocessing.PolynomialFeatures.html>

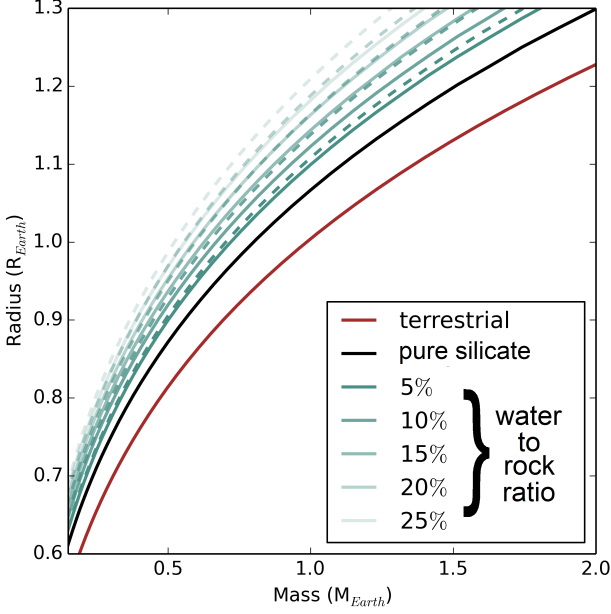


Fig. A.2. Comparisons of mass-radius relationships for water-rich planets (with water in condensed phase) of Zeng et al. (2016) (solid blue lines) with mass-radius relationships calculated in the present work (dashed blue lines), and assuming a layer of condensed water is added on top of mass-radius relationships for pure silicate (MgSiO_3) planets of Zeng et al. (2016).

As a third step, we used the recursive feature elimination (RFE) iterative method (Pedregosa et al. 2011) to derive the optimal polynomial fit of our data, using the RFE python tool⁷. The RFE method was implemented following the recursive steps described below, for each n (from $n = 8$ to 1):

1. We performed a linear fit of our modeled data (surface temperature and effective temperature) with the polynomial of N terms (initially, and for reference, $N = \frac{(k+n)!}{n! k!}$).
2. We calculated the RMS of the fit.
3. We evaluated the absolute contribution of all N polynomial terms to the fit.
4. We removed the polynomial term with the smallest absolute contribution.
5. We restarted the procedure iteratively with $N-1$ terms, and until $N = 1$.

As the final step, we compared the RMS of the fit for each polynomial in order to derive the best compromise between the value of the RMS and the number N of polynomial terms. Based on Fig. B.1, we decided that the fit that gives the best compromise is found for $N = 10$ for both the surface temperature and the effective temperature. Fig. B.1 shows the distribution of the residuals of the fit for the surface temperature and the effective temperature, thus making it possible to evaluate the goodness of the fit (mean error $\sim 2.5\%$; max error $\sim 10\%$).

⁷ https://scikit-learn.org/stable/modules/generated/sklearn.feature_selection.RFE.html

Appendix C: Procedure to derive the empirical formula of the thickness of a steam H_2O atmosphere

To construct Equation 2, we first assumed the hydrostatic equilibrium:

$$dP + \rho g dr = 0, \quad (\text{C.1})$$

with P the atmospheric pressure, r the radial coordinate, g the gravity, and r the radial coordinate. g can be written as

$$g(r) = g_{\text{core}} \times \left(\frac{R_{\text{core}}^2}{r^2} \right). \quad (\text{C.2})$$

We then assumed the atmosphere follows the perfect gas law:

$$\rho = \frac{P M_{\text{H}_2\text{O}}}{R T_{\text{eff}}}, \quad (\text{C.3})$$

with R the gas constant and $M_{\text{H}_2\text{O}}$ the molecular weight of H_2O (here the dominant gas). T_{eff} is the effective atmospheric temperature and assumed to be constant, for simplicity.

Combining the three previous equations, we derived:

$$d(\log P) = \left(\frac{M_{\text{H}_2\text{O}} g_{\text{core}}}{R T_{\text{eff}}} \right) R_{\text{core}}^2 d\left(\frac{1}{r}\right). \quad (\text{C.4})$$

We then integrated this equation (assuming $P = P_{\text{surf}}$ at $r = R_{\text{core}}$):

$$\log\left(\frac{P}{P_{\text{surf}}}\right) = \left(\frac{M_{\text{H}_2\text{O}} g_{\text{core}}}{R T_{\text{eff}}} \right) \times R_{\text{core}}^2 \times \left(\frac{1}{r} - \frac{1}{R_{\text{core}}} \right). \quad (\text{C.5})$$

At the transit radius, $R = R_p$ and $P = P_{\text{transit}}$, which gives

$$\log\left(\frac{P_{\text{transit}}}{P_{\text{surf}}}\right) = \left(\frac{M_{\text{H}_2\text{O}} g_{\text{core}}}{R T_{\text{eff}}} \right) \times R_{\text{core}}^2 \times \left(\frac{1}{R_p} - \frac{1}{R_{\text{core}}} \right), \quad (\text{C.6})$$

which can be rewritten as

$$R_p = \left(\left(\frac{R T_{\text{eff}}}{M_{\text{H}_2\text{O}} g_{\text{core}}} \right) \times \left(\frac{1}{R_{\text{core}}^2} \right) \times \log\left(\frac{P_{\text{transit}}}{P_{\text{surf}}}\right) + \frac{1}{R_{\text{core}}} \right)^{-1}. \quad (\text{C.7})$$

With $R_p = R_{\text{core}} + z_{\text{atmosphere}}$, we have

$$z_{\text{atmosphere}} = R_{\text{core}} \left(\frac{R_{\text{core}}}{\log\left(\frac{P_{\text{surf}}}{P_{\text{transit}}}\right) \left(\frac{R T_{\text{eff}}}{M_{\text{H}_2\text{O}} g_{\text{core}}} \right)} - 1 \right)^{-1}. \quad (\text{C.8})$$

We then assumed

$$P_{\text{surf}} = \frac{M_{\text{atmosphere}} g_{\text{core}}}{4\pi R_{\text{core}}^2}, \quad (\text{C.9})$$

with $M_{\text{atmosphere}}$ the mass of the steam H_2O -dominated atmosphere (in kg). This relationship does not hold for inflated atmospheres, but for simplicity, we assumed it is valid anyway. Moreover, we have

$$M_{\text{atmosphere}} = \frac{M_{\text{core}} x_{\text{H}_2\text{O}}}{1 - x_{\text{H}_2\text{O}}} = \frac{g_{\text{core}} R_{\text{core}}^2}{G} \times \left(\frac{x_{\text{H}_2\text{O}}}{1 - x_{\text{H}_2\text{O}}} \right). \quad (\text{C.10})$$

Combining the three previous equations leads to Equation 2.

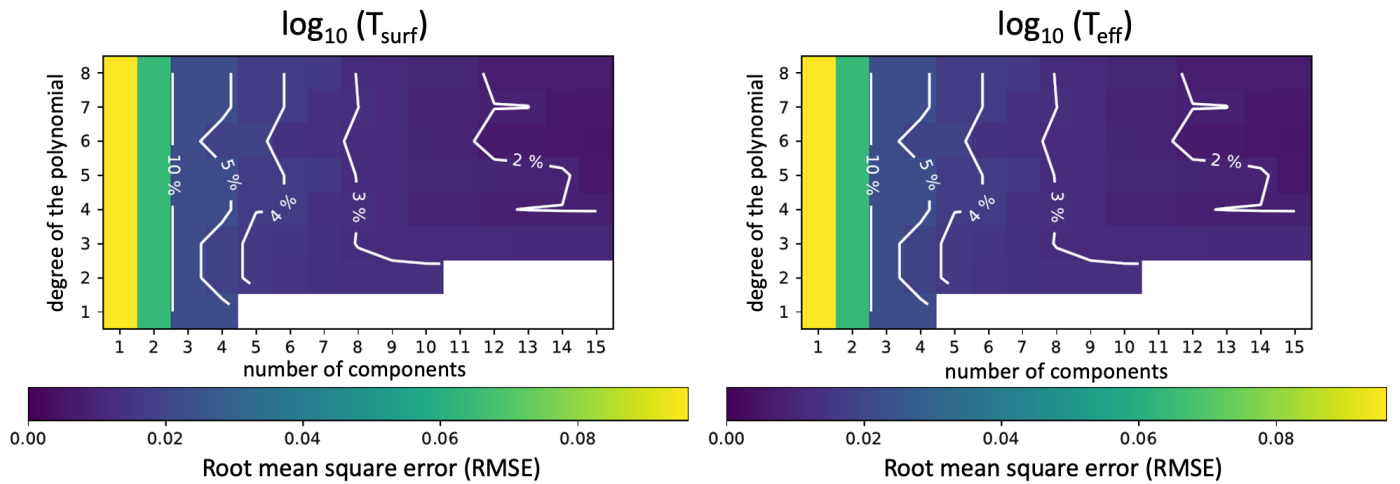


Fig. B.1. Maps of the root mean square error (RMSE) for the fits on the surface temperature T_{surf} (left panel) and the effective temperature T_{eff} (right panel), as a function of the number of polynomial components and the initial degree of the polynomial.

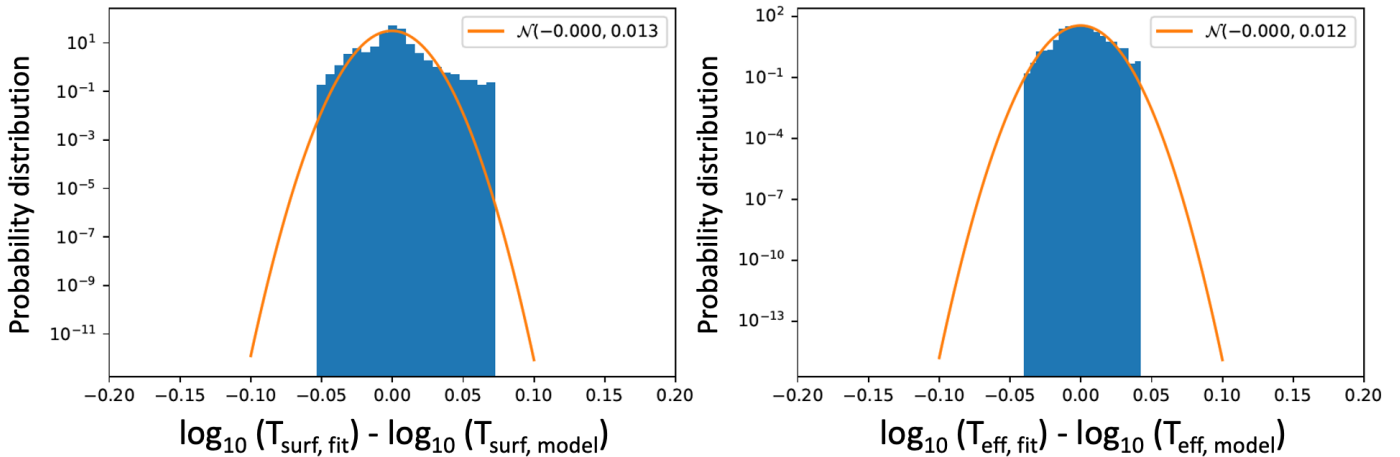


Fig. B.2. Probability distributions (blue histogram) of residuals for the fits on the surface temperature T_{surf} (left panel) and the effective temperature T_{eff} (right panel). A total of 16488 1-D numerical atmospheric simulations were used. The orange curves indicate the normal distribution laws that best fit the distributions.

Appendix D: Quick guide on how to build mass-radius relationships for water-rich rocky planets more irradiated than the runaway greenhouse limit.

In this Appendix, we provide a procedure that can be followed to build mass-radius relationships for water-rich rocky planets more irradiated than the runaway greenhouse limit:

1. Choose a core composition.
2. Retrieve (or calculate) the mass-radius relationship corresponding to this core composition. For instance, Zeng et al. (2016)⁸ provides ascii tables of mass-radius relationships for a wide range of interior composition.
3. Choose the water mass fraction ($x_{\text{H}_2\text{O}}$) of your planets, as well as the irradiation (S_{eff}) they receive. We note that the irradiation must be larger than the runaway greenhouse irradiation limit, which depends on the type of host star (Kopparapu et al. 2013) and on the mass and radius of the planetary core (Kopparapu et al. 2014). Moreover, the water mass fraction must be "reasonable" (see discussions in Appendix A).
4. For each datapoint of the selected core mass-radius relationship (i.e., for each set of core mass and radius), calculate the corresponding surface gravity (g_{core}).
5. For each datapoint of the selected core mass-radius relationship, compute the thickness $z_{\text{atmosphere}}$ of the H_2O atmospheric layer using Equation 2. Equation 2 makes use of Equation 3 and the empirical coefficients provided in Table 2.
6. For each datapoint of the selected core mass-radius relationship ($M_{\text{core}}, R_{\text{core}}$), compute the new mass-radius relationship ($M_{\text{planet}}, R_{\text{planet}}$) by assuming that $R_{\text{planet}} = R_{\text{core}} + z_{\text{atmosphere}}$ and $M_{\text{planet}} = M_{\text{core}} / (1 - x_{\text{H}_2\text{O}})$.

⁸ User-friendly data is provided on the personal website of Li Zeng (<https://www.cfa.harvard.edu/~lzeng/planetmodels.html>)